ALE beam using reference dynamics

Kilian Grundl[1] · **Thorsten Schindler**[1] ·
Heinz Ulbrich[1] · **Daniel J. Rixen**[1]

Abstract We present a small strain beam model based on the Arbitrary Lagrangian Eulerian setting for use in multibody dynamics. The key contribution of the present paper is to provide a formulation with large flexible reference motion and small overlaid deflections. We point out that the reference motion is described by actual degrees of freedom of the model. Therefore, we use a vector of generalized positions and an Eulerian coordinate, which itself is a degree of freedom and in which the flow of the beam material through an arbitrary volume is represented. The additional displacements describe small fluctuations around the reference motion. With this idea it is easy to separate the motion of belt drives, cable and rope ways or strings. In particular, the overlaid deflections are described for efficient numeric computation and may be analyzed in an easy way for vibrational behavior. The guiding reference motion is arbitrary, i.e., the transmission ratios are degrees of freedom and may change dynamically affecting also the fluctuations. Contacts with dry friction are foreseen and represented in the present model. It is validated and proven to be efficient in comparison with classic co-rotational and absolute nodal coordinate formulations in our application. The simulation of pushbelt continuously variable transmissions is taken as a high-dimensional industrial example.

✉ K. Grundl
kilian.grundl@tum.de

T. Schindler
thorsten.schindler@mytum.de

H. Ulbrich
ulbrich@tum.de

D.J. Rixen
rixen@tum.de

[1] Institute of Applied Mechanics, Technische Universität München, Garching bei München, Germany

1 Introduction

Beams are defined as flexible structures with one dimension much larger than the other two dimensions. The respective theory provides fast models for the dynamic simulation in comparison with the direct application of general finite element (FE) models. The decoupling into linear cross-section evaluations and nonlinear center line kinematics is usually based on a small strain assumption [4, 15].

The application of beam models is still crucial within multibody systems, which is proven by recent publications mainly about geometrically exact descriptions [36] dating back to the pioneering work of Simo [34, 35]. An overview of flexible multibody systems is given in the paper of Wasfy [40] or the one of Shabana [33]. Both classify beam formulations concerning specific criteria. Wasfy distinguishes the floating frame of reference formulation [31, 32], co-rotated formulations [6, 9], and inertial formulations [3] as mathematical descriptions of the continuum equations. Shabana's view is approximation based. He considers the incremental FE method, the finite segment method, i.e., lumped mass superelements, large rotation vector formulations, and absolute nodal coordinate formulations (ANCF) [10, 16, 31, 32]. Geometrically exact beams belong to the large rotation vector formulations [19, 20, 39]. A comparison between geometrically exact beams and ANCF beams is given in [25].

Nonlinear elasticity in general is summarized in Antman's book [2]. In particular, geometrically nonlinear problems are characterized by nonlinear strain–displacement relationships related to large displacement gradients found when the body undergoes large rotations or large deformations. The right mathematical formulation and approximation has to be picked. For beams, some are mentioned in the previous paragraph.

The equations of motion (EOMs) of multibody systems are nonlinear in general even for linear elastic material because of the large overall motion. The choice of how to model a specific example application is crucial and depends not only on strains and displacements in the system. External loads can cause effects which can directly be included in the model, cf. centrifugal stiffening phenomena in helicopter blades. The properties of the cross section highly influence the behavior of the beam especially for laminated composite materials and are often calculated in a pre-processing step [4]. In the case of contacts, locality of the deformation has to be preserved [41, 43].

In this paper, we present a description of beams specifically suited for belt drives [26, 29, 30, 42]. We are interested in an efficient way to model the geometrically nonlinear and transient motion in an overall small strain setting. We describe the reference motion and add overlaid small deflection, which can be interpreted as a linearization about the changing reference state. The EOMs for a one-dimensional closed continuum are derived using an Eulerian view. The tangential movement of a mass particle is projected to a fixed position in space to focus on the vibrations and the transient and nonlinear behavior of the reference curve, e.g. due to changing transmission ratios. As we model the frictional interactions with arbitrary bodies [1, 23], the Lagrangian view following the mass particles is necessary for the derivation of the overall equations. Using the Arbitrary Lagrangian Eulerian (ALE) transformation, we meet all requirements. The EOMs are derived with the Lagrange II formalism, which may be stated in the general language of Irschik and Holl [18], but they are derived from scratch in a simple setting also in the present paper. In general, the sliding beam problem is quite popular. Behdinan [5] describes two different formulations starting from Hamilton's principle. Vetyukov [37, 38] gives an overview with belt and plate examples based on a fixed reference kinematics and prescribed guiding velocity, whereby we also refer to the literature therein. Also in [12] and [11], the reference kinematics of belt drive is fixed. A well-known application of the Eulerian view is the Spaghetti problem of VuQuoc [39]. We

refer in particular to the ALE-technique used by Pechstein and Gerstmayr in combination with ANCF elements for a planar belt model with a fixed reference shape [22] as it motivated our work. However, in contrast, we propose a model for belt drives with a non-fixed reference shape that dynamically undergoes large changes such as the variation of pulley radius in a continuously variable transmission (CVT). These changes are modeled with an extra set of (reference) degrees of freedom (DOFs), in particular the transformation parameter between Eulerian and Lagrangian coordinate space. Our model uses planar reference motion but includes spatial, overlaid deformation. We verify the general behavior of the model and show inherent properties using numerical tests.

The model is difficult to place in the classification of Wasfy. The reference motion is an inertial description, whereas the overlaid deformation shows characteristics of a floating frame or co-rotational approach. In this sense, it is a specific model to deal with the high demands in belt drive systems. In particular, the new development is motivated by reducing the computation time for a large pushbelt CVT simulation model [26, 28, 30]. The belt speed and the transmission ratio define the DOFs of the reference motion. We compare simulation results and computation time for several beam elements used in the pushbelt CVT so far (classic absolute nodal coordinate beams [10] and redundant coordinate methods [26, 30, 41, 43], i.e., co-rotational descriptions). We highlight the performance of the new model concerning the mentioned criteria in the designated application. This paper extends the ideas that are presented in [17, Chap. 2]. Essentially we introduce a new theory that models a system with a reference curve, which allows us to approximate the behavior of a complex dynamic system much more efficiently.

The outline of the paper is as follows. First, we derive the EOMs for a one-dimensional closed continuum in the Eulerian view. Next, we deduce the position and velocity formulas for the center line of the beam model using the idea of a reference motion. We show the generalized forces in the case of a planar reference motion and apply the equations to an industrial example. We derive the specific reference motion for the system 'pushbelt CVT'and test the model numerically in academic settings. Finally, we compare the outputs in an overall model with other beam models to prove the applicability and efficiency of the new model. After the summary, we list possible considerations for improvements and applications.

2 Lagrange equations for an Eulerian description of a one-dimensional closed continuum

In the following, the transformation between the Eulerian description and the Lagrangian description is outlined and the related Lagrange equations are written for a one-dimensional case. Irschik and Holl deduce the equations [18] for the general case. Our derivation holds for a closed one-dimensional continuum.

2.1 Preliminaries

Figure 1 describes the relation between the material Lagrangian coordinate $\bar{x}$ and the respective spatially fixed Eulerian observer location ξ along a curve with fixed length, i.e., assuming no stretching along the one-dimensional curve, i.e., only a homogeneous speed $\dot{s}$. In other words, the displacement along the curve $s(t)$ (a scalar) is assumed to depend only on time t.

The Eulerian coordinate ξ along the continuum defines a point fixed in space. The Lagrangian coordinate $\bar{x}$ along the continuum follows the particle over time and can also be

Fig. 1 Spatially fixed Eulerian
observer coordinate ξ and
material Lagrangian coordinate $\bar{x}$

$$\xi = \bar{x} + s$$
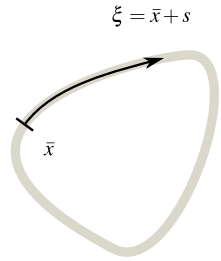
understood as the spatial position of the material point if the displacement would be null.
Hence, the observer position ξ is reached by $\bar{x}$ with the displacement $s(t)$, assuming a uniform curvilinear velocity:

$$\bar{x} = \xi - s(t) \tag{1}$$

and we can write

$$\frac{\partial \bar{x}}{\partial \xi} = 1, \qquad \frac{\partial \bar{x}}{\partial s} = -1, \qquad \frac{d\bar{x}}{dt} = -\frac{ds}{dt} = -\dot{s}, \tag{2}$$

where we assume that the observation location ξ does not move.

If we define a function f as an integral of an arbitrary function $g(\bar{x}, t)$ over time depending limits $l = l(t), u = u(t)$ as

$$f := \int_l^u g(\bar{x}, t) d\bar{x} \,,$$

the absolute time derivative of f is given by the Leibniz integral rule:

$$\begin{aligned}
\frac{df}{dt} &= \frac{\partial f}{\partial l} \frac{dl}{dt} + \frac{\partial f}{\partial u} \frac{du}{dt} + \int_l^u \frac{dg}{dt} d\bar{x} \\
&= -g(l, t) \frac{dl}{dt} + g(u, t) \frac{du}{dt} + \int_l^u \frac{\partial g}{\partial \bar{x}} \frac{d\bar{x}}{dt} d\bar{x} + \int_l^u \frac{\partial g}{\partial t} d\bar{x},
\end{aligned} \tag{3}$$

where d symbolizes the absolute derivative and ∂ the partial derivative.

2.2 Closed curve

For a closed one-dimensional structure, the integral limits as well as the inner function evaluation change equally over time:

$$\frac{dl}{dt} = \frac{du}{dt} \quad \text{and} \quad g(l, t) = g(u, t).$$

Hence, the first two terms in (3) vanish. Further, the first integral of (3) is zero as well since

$$-\int_l^u \dot{s} \frac{\partial g}{\partial \bar{x}} d\bar{x} = -\dot{s}\big(g(u, t) - g(l, t)\big) = 0.$$

A transformation of variables to integrate along ξ with $u = L - s$ and $l = 0 - s$ and the length L of the continuum yields

$$\frac{df}{dt} = \int_0^L \frac{\partial g}{\partial t} d\xi. \tag{4}$$

2.3 Energy expressions

The EOMs can be derived considering the Lagrangian $\mathscr{L} = \mathscr{T} - \mathscr{V}$ and the standard Lagrange II equation (e.g. [24])

$$\frac{d}{dt} \frac{\partial \mathscr{L}}{\partial \dot{q}_k} - \frac{\partial \mathscr{L}}{\partial q_k} = 0$$

where q_k index the generalized DOFs of the model and $\dot{q}_k$ their time derivatives and where we assume all forces deriving from a potential $\mathscr{V}$. The kinetic energy is defined as

$$\mathscr{T} = \frac{1}{2} \int_\Omega v^T v \rho d\Omega = \frac{1}{2} \rho \int_\Omega v^T v d\Omega \tag{5}$$

where Ω is the reference (undeformed) volume for the integration, ρ is the constant density of the undeformed material and v the absolute velocity field. Considering the one-dimensional continuum to be a beam-like structure, we can further write

$$\mathscr{T} = \frac{1}{2} \rho A \int_l^u v^T v d\bar{x} = \frac{1}{2} \rho A \int_0^L v^T v d\xi \tag{6}$$

where we neglect the energy related to the rotation of the cross section and where A denotes the area of the cross section. The expression for the Lagrange II equation results in

$$\frac{d}{dt} \frac{\partial \mathscr{T}}{\partial \dot{q}_k} - \frac{\partial \mathscr{T}}{\partial q_k} = Q_k \quad \text{and} \quad Q_k =: -\frac{\partial \mathscr{V}}{\partial q_k}. \tag{7}$$

Using (4) and (6), it follows

$$\frac{d}{dt} \frac{\partial \mathscr{T}}{\partial \dot{q}_k} = \frac{\rho A}{2} \int_0^L \frac{\partial}{\partial t} \frac{\partial (v^T v)}{\partial \dot{q}_k} d\xi. \tag{8}$$

Observe that the limits of the integral do not depend on the generalized velocities $\dot{q}_k$. The derivative of the kinetic energy with respect to the generalized positions follows analogously:

$$\frac{\partial \mathscr{T}}{\partial q_k} = \frac{\rho A}{2} \int_0^L \frac{\partial (v^T v)}{\partial q_k} d\xi. \tag{9}$$

As the potential energy can be generally represented as an integral over a function $g_{\mathscr{V}}$, yet to be defined, it follows

$$\mathscr{V} := \int_l^u g_{\mathscr{V}} d\bar{x} \quad \text{with} \quad \frac{\partial \mathscr{V}}{\partial q_k} = \int_0^L \frac{\partial g_{\mathscr{V}}}{\partial q_k} d\xi ,$$

which gives the last term in (7).

All expressions are written using Eulerian description. For the special case of a closed beam structure, the ALE-transformation does not yield additional terms compared to the Lagrange setting.

3 Kinematics

The general equations of the previous section are applied to a belt drive, i.e., a closed beam in the following. In order to clarify how the deformations in the belt will be later approximated, we start this section by introducing the shape functions that will determine the kinematics of the centerline of the belt. The displacement of the belt will first be represented by an overall shape that is parametrized by DOFs governing the reference shape of the unstretched belt. Around that reference configuration, additional displacements – assumed to remain small – are allowed by introducing deformation shape functions. These allow the belt to have a general displacement, to also stretch and have additional perturbation in the binormal directions to the reference shape.

3.1 Position

Consider a belt drive with a fixed belt length L (Fig. 2). A reference curve $r_{Ref}(\xi, q_R)$ is described along $\xi \in [0, L[$ in an inertial frame with axes x, y and z. The current reference curve of the elastic centerline may depend on the m DOFs q_R. On each reference position, a frame is attached holding the tangential t_{Ref}, normal n_{Ref} and binormal b_{Ref}. A tangential drift s defines the position of a particle along the curve. The reference motion is described with the degrees of freedom s and q_R. Additional n DOFs q_f are introduced which enable a small displacement r_f of the centerline around the reference position r_{Ref} (Fig. 3). The vector q_f holds the DOFs q_{fi} which describe the local deviation at certain nodes in the three possible spatial directions. Local trial function vectors $\mathbb{S}_i(\xi) \in \mathbb{R}^3$ span the local deformation field r_f in-between the nodes. The position of a particle is given by

$$r = r_{Ref} + r_f = r_{Ref} + \sum_{i=1}^{n} \mathbb{A}_i \mathbb{S}_i q_{fi} = r_{Ref} + \mathbb{B} q_f \tag{10}$$

where $\mathbb{A}_i(\xi, q_R)$ is introduced as a general transformation matrix for the displacements $\mathbb{S}_i q_{fi}$ from a local frame for DOFs q_{fi} to the global one. Two possibilities to choose $\mathbb{A}_i$ are discussed in this paper:

1. The most simple option is to choose a constant $\mathbb{A}_i$, e.g. as the identity matrix. It does neither depend on ξ nor on q_R. The trial functions interpolate the q_{fi} in an inertial frame.

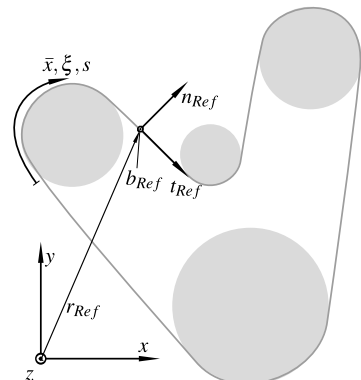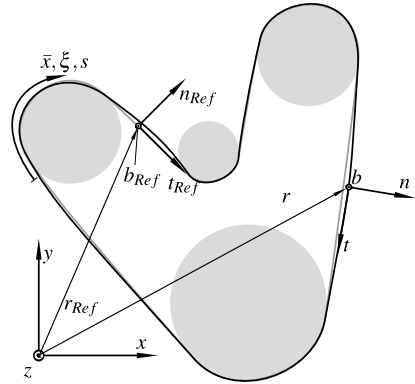**Fig. 2** Reference curve

Fig. 3 Reference curve with deformations

2. The most general option is to choose $\mathbb{A}_i$ to depend on q_R and ξ. It could be defined as the orientation matrix $\mathbb{A}_i = [t_{Ref}, n_{Ref}, b_{Ref}]$ which changes over the arc with ξ. The local DOFs can be interpreted in the direction of the local tangential, normal and binormal direction along the whole curve, respectively.

We derive the equations for this general, second case, i.e., $\mathbb{B}(\xi, q_R)q_f := \sum_{i=1}^{n} \mathbb{A}_i(\xi, q_R)\mathbb{S}_i q_{fi}$.

3.2 Velocity

To get the absolute velocity, the material derivative[1] has to be applied[2] with

$$v = \frac{\mathrm{d}r}{\mathrm{d}t} = \frac{\mathrm{d}r_{Ref}}{\mathrm{d}t} + \frac{\mathrm{d}\mathbb{B}}{\mathrm{d}t}q_f + \mathbb{B}\frac{\mathrm{d}q_f}{\mathrm{d}t}$$

$$= \frac{\partial r_{Ref}}{\partial \xi}\dot{s} + \frac{\partial r_{Ref}}{\partial q_R}\dot{q}_R + \frac{\partial \mathbb{B}}{\partial \xi}\dot{s}q_f + \left(\frac{\partial \mathbb{B}}{\partial q_R}\dot{q}_R\right)q_f + \mathbb{B}\dot{q}_f$$

which can be rearranged as

$$v = \frac{\partial r}{\partial \xi}\dot{s} + \frac{\partial r}{\partial q_R}\dot{q}_R + \mathbb{B}\dot{q}_f.$$

Using the vectors of generalized coordinates and generalized velocities

$$q^T = \begin{bmatrix} s & q_R & q_f \end{bmatrix}, \qquad \dot{q}^T = \begin{bmatrix} \dot{s} & \dot{q}_R & \dot{q}_f \end{bmatrix} \tag{11}$$

the velocity can be written as

$$v = \mathbb{P}\dot{q} \quad \text{where } \mathbb{P}(q) := \begin{bmatrix} r' & \frac{\partial r}{\partial q_R} & \mathbb{B} \end{bmatrix} \tag{12}$$

---

[1]The absolute change in the position of a mass particle is derived based on $r(\bar{x})$ with $\bar{x}$ being constant (cf. (2)).

[2]The derivative of a matrix $\mathbb{G}$ w.r.t. to a vector d applied to a vector e is defined as

$$\frac{\mathrm{d}\mathbb{G}}{\mathrm{d}d}e = \sum_{i=1}^{k} \frac{\mathrm{d}\mathbb{G}}{\mathrm{d}d_i}e_i$$

where d and e have the dimension k.

is the interpolation matrix between the generalized velocities $\dot{q}$ and the velocity of the mass particles. It depends solely on the generalized positions q. Prime $'$ defines the derivative with respect to ξ. We want to emphasize that besides q_R and q_f also s is a degree of freedom of the model.

4 Equations of motion and generalized forces

In the following, we set-up the generalized forces. The terms resulting from the kinetic energy are derived directly from the kinematical description which holds for the general spatial case. We choose a reference motion in the xy-plane. Thus, the reference position r_{Ref} is planar and the overlaid small deformation r_f introduces an arbitrary spatial motion. For the elastic energy, a standard homogeneous material is used which is suitable for many applications. Advanced constitutive laws may be applied in a straightforward manner depending on the application.

4.1 Kinetic energy

The gradient of the kinetic energy with respect to the generalized coordinates is given by

$$\frac{\partial \mathscr{T}}{\partial q} = \rho A \int_0^L v^T \frac{\partial v}{\partial q} d\xi = \rho A \dot{q}^T \mathbb{I}_{PTdPdq} \dot{q} \tag{13}$$

where the integral

$$\mathbb{I}_{PTdPdq} := \int_0^L \mathbb{P}^T \frac{\partial \mathbb{P}}{\partial q} d\xi$$

has to be evaluated in each time step.

The time derivative of the gradient of the kinetic energy with respect to the generalized velocities is

$$\frac{d}{dt} \frac{\partial \mathscr{T}}{\partial \dot{q}} = \frac{\rho A}{2} \int_0^L \frac{\partial}{\partial t} \frac{\partial}{\partial \dot{q}} (v^T v) d\xi = \frac{\rho A}{2} \int_0^L 2 \frac{\partial}{\partial t} \left(v^T \frac{\partial v}{\partial \dot{q}} \right) d\xi = \rho A \int_0^L \frac{\partial}{\partial t} (\dot{q}^T \mathbb{P}^T \mathbb{P}) d\xi$$

$$= 2 \rho A \dot{q}^T \mathbb{I}_{PTdPdt} + \ddot{q}^T \rho A \mathbb{I}_{PTP} \tag{14}$$

where the first integral is defined as

$$\mathbb{I}_{PTdPdt} := \int_0^L \mathbb{P}^T \frac{\partial \mathbb{P}}{\partial t} d\xi \tag{15}$$

and the second term yields the symmetric mass matrix

$$\mathbb{M} := \rho A \mathbb{I}_{PTP} := \rho A \int_0^L \mathbb{P}^T \mathbb{P} d\xi. \tag{16}$$

The time derivative is written as a partial time derivative according to (4): this includes the indirect dependency hidden in the generalized coordinates.

4.2 Elastic energy

In this work, we assume the belt to be slender for the bending around both normal directions so that the Kirchhoff–Bernoulli assumptions can be applied: cross sections remain plane and orthogonal to the elastic centerline. The shear deformation is thus assumed to be null so that the deformation energy originates only from tangential stretching and bi-axial bending described by the local curvatures. The stretching originates only from the deformation shape function of the centerline, whereas the curvature and associated bending are generated both by the reference shape and the additional deformation.

The elastic energy $\mathscr{V}$ is defined following [19] with

$$\mathscr{V} := \frac{1}{2} \int_0^L \gamma^T \mathbb{C}_\gamma \gamma \, d\xi + \frac{1}{2} \int_0^L \kappa^T \mathbb{C}_\kappa \kappa \, d\xi = \mathscr{V}_\gamma + \mathscr{V}_\kappa \tag{17}$$

where γ and κ are measures for the strains related to deformations originating from translation and rotational deformation, respectively, and the matrices $\mathbb{C}_\gamma$ and $\mathbb{C}_\kappa$ contain the related beam stiffnesses. The partial derivatives are given by

$$\frac{\partial \mathscr{V}_\gamma}{\partial q} = \int_0^L \gamma^T \mathbb{C}_\gamma \frac{\partial \gamma}{\partial q} d\xi \quad \text{and} \quad \frac{\partial \mathscr{V}_\kappa}{\partial q} = \int_0^L \kappa^T \mathbb{C}_\kappa \frac{\partial \kappa}{\partial q} d\xi \tag{18}$$

with the normal strain energy $\mathscr{V}_\gamma$ and the bending strain energy $\mathscr{V}_\kappa$. We assume the material to be linear elastic and isotropic and that the deformations can be measured in the principal axis. With the Young modulus E and the cross section A as well as the moments of inertia for bending I_n and I_b in normal and binormal direction, respectively, the constitutive laws follow as

$$\mathbb{C}_\gamma = EA \quad \text{and} \quad \mathbb{C}_\kappa = \begin{bmatrix} EI_n & 0 \\ 0 & EI_b \end{bmatrix}. \tag{19}$$

Torsion is not incorporated in this paper. In our application the out-of-plane deformation in the direction of the binormal b is small and therefore torsion is negligible. Furthermore, we observed numerically unfavorable behavior due to torsion in our system [26]. The small out-of-plane motion in binormal direction is incorporated to show the extensibility to the general spatial case, which is successfully applied in [17].

For the normal strain energy the material strain measure is used with

$$\gamma = t^T r' - 1 \tag{20}$$

where the local tangential t direction of the center line follows the Frenet formulas, which also define the local[3] directions of the normal and binormal.

$$t = \frac{r'}{\|r'\|} = n \times b, \qquad n = \frac{t'}{\|t'\|} = b \times t \quad \text{and} \quad b = \frac{r' \times t'}{\|r'\| \|t'\|} = t \times n. \tag{21}$$

With this definition of the tangential direction t, the Kirchhoff assumption is fulfilled. The cross section is not able to rotate relatively to the neutral phase [20, Remark 3.4]. Using Kirchhoff beam theory is advantageous compared for instance to a Timoschenko model

---

[3][t n b] refers to the local deformations and does not coincide with $[t_{Ref} \ n_{Ref} \ b_{Ref}]$.

since, when discretized by finite elements, the latter can exhibit locking unless proper reduced integration is used. The normal strain energy follows as

$$\frac{\partial \mathcal{V}_\gamma}{\partial q} = EA \int_0^L (r'^T t - 1) \frac{\partial}{\partial q_k} (t^T r') d\xi$$

$$= EA \int_0^L (\sqrt{r'^T r'} - 1) \frac{\partial}{\partial q_k} \sqrt{r'^T r'} d\xi$$

$$= EA \int_0^L (\sqrt{r'^T r'} - 1) \frac{1}{\sqrt{r'^T r'}} r'^T \frac{\partial}{\partial q_k} r' d\xi$$

and it is finally given by

$$\frac{\partial \mathcal{V}_\gamma}{\partial q} = EA \int_0^L \left(1 - \frac{1}{\sqrt{r'^T r'}}\right) r'^T \begin{bmatrix} \begin{bmatrix} 0 \\ 0 \\ 0 \end{bmatrix} & \frac{dr'}{dq_R} & \mathbb{B}'_1 & \cdots & \mathbb{B}'_n \end{bmatrix} d\xi =: EA\mathbb{I}_{\mathcal{V}\gamma}.$$

The bending measures are defined as

$$\kappa := \begin{pmatrix} \kappa_n \\ \kappa_b \end{pmatrix} \tag{22}$$

where κ_n and κ_b measure the curvatures in the two planes that are spanned between the tangential vector t_{Ref} and the normal n_{Ref} or the binormal b_{Ref}, respectively. The energy derivatives follow as

$$\frac{\partial \mathcal{V}_\kappa}{\partial q} = EI_n \int_0^L \kappa_n \frac{\partial}{\partial q} \kappa_n d\xi + EI_b \int_0^L \kappa_b \frac{\partial}{\partial q} \kappa_b d\xi =: EI_n \mathbb{I}_{\mathcal{V}n} + EI_b \mathbb{I}_{\mathcal{V}b}.$$

The single measures are discussed in the following.

For the curvature in the t_{Ref}/n_{Ref}-plane, it is crucial to couple the reference deformation and the overlaid effects. Only due to this, the full physics of the beam can be represented. Otherwise, the elastic forces of the reference DOFs would only affect the reference motion, i.e., the forces would not be projected into the generalized direction of the overlaid DOFs. With the illustrative example of a circle-like deformation-free state, a damped dynamic simulation starting from an arbitrary initial state would not result in the circular shape in the case of no external forces if the coupling of reference and overlaid motion has not been covered in the right way (see Sect. 5.3). To approximate the curvature in the t_{Ref}/n_{Ref}-plane, the second derivative of the position is projected along the reference normal direction:

$$\kappa_n := n_{Ref}^T r'' \quad \text{with } r'' = r''_{Ref} + \mathbb{B}'' q_f.$$

This approximation yields correct measures for the reference part and linearized overlaid measures for the additional deformations. The derivatives with respect to the generalized coordinates are

$$\frac{\partial}{\partial s} \kappa_n = 0, \tag{23a}$$

$$\frac{\partial}{\partial q_R} \kappa_n = \frac{\partial n_{Ref}^T}{\partial q_R} r'' + n_{Ref}^T \frac{\partial r''}{\partial q_R}, \tag{23b}$$

$$\frac{\partial}{\partial q_{fi}}\kappa_n = n_{Ref}^T \frac{\partial r_f''}{\partial q_{fi}} = n_{Ref}^T\left(\mathbb{A}_i''\mathbb{S}_i + 2\mathbb{A}_i'\mathbb{S}_i' + \mathbb{A}_i\mathbb{S}_i''\right). \tag{23c}$$

Analogously, the binormal curvature measure in the t_{Ref}/b_{Ref}-plane is approximated as

$$\kappa_b := b_{Ref}^T r''$$

where derivatives with respect to the generalized coordinates follow with

$$\frac{\partial}{\partial s}\kappa_b = 0, \tag{24a}$$

$$\frac{\partial}{\partial q_R}\kappa_b = \underbrace{\frac{\partial b_{Ref}^T}{\partial q_R}}_{=0} r'' + b_{Ref}^T \frac{\partial r''}{\partial q_R}, \tag{24b}$$

$$\frac{\partial}{\partial q_{fi}}\kappa_b = b_{Ref}^T \frac{\partial r_f''}{\partial q_{fi}} = b_{Ref}^T\left(\mathbb{A}_i''\mathbb{S}_i + 2\mathbb{A}'\mathbb{S}_i' + \mathbb{A}\mathbb{S}_i''\right) = \begin{bmatrix} 0 & 0 & 1 \end{bmatrix}\mathbb{S}_i''. \tag{24c}$$

4.3 External forces

External forces from joints or contacts have to be projected into the generalized directions. The Jacobian of translation has to be found which relates the global free directions with the generalized directions. According to (12), it is the transformation matrix $\mathbb{P}$:

$$J_T := \frac{\partial v}{\partial \dot{q}} = \mathbb{P}.$$

Interaction torques have to be modeled as force pairs.

4.4 Equations of motion

Summarizing the previous findings, we gain the EOMs

$$\mathbb{M}\ddot{q} = h \tag{25}$$

where the mass matrix is defined by (16) and the right hand side vector h follows with two parts of the kinetic energy and three parts of the potential energy.

$$h = h_{\mathscr{T}1} + h_{\mathscr{T}2} + h_{\mathscr{V}1} + h_{\mathscr{V}2} + h_{\mathscr{V}3}, \tag{26a}$$

$$h_{\mathscr{T}1} = -2\rho A\dot{q}^T\mathbb{I}_{PTdPdt}, \tag{26b}$$

$$h_{\mathscr{T}2} = \rho A\dot{q}^T\mathbb{I}_{PTdPdq}\dot{q}, \tag{26c}$$

$$h_{\mathscr{V}1} = -EA\mathbb{I}_{\mathscr{V}\gamma}, \tag{26d}$$

$$h_{\mathscr{V}2} = -EI_n\mathbb{I}_{\mathscr{V}n}, \tag{26e}$$

$$h_{\mathscr{V}3} = -EI_b\mathbb{I}_{\mathscr{V}b}. \tag{26f}$$

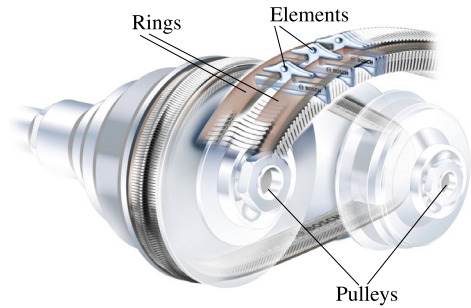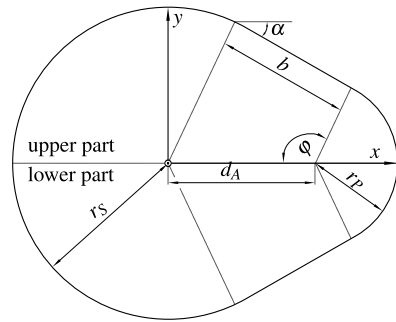**Fig. 4** Pushbelt CVT. ©Bosch Transmission Technology

Fig. 5 Kinematics of a simple reference curve

5 Example: continuously variable transmission

We prove the applicability of the derived model within the framework of multibody simulation in this section. The beam model is applied within a pushbelt CVT system (Fig. 4). The CVT transmits torque and power between two pulleys. Its conical sheaves clamp the pushbelt on the steel element flanks. The ratio between the clamping forces on the primary and secondary pulley-arcs determine the transmission ratio. In-between the elements a push force acts due to the applied torque on the pulleys. The elements guided by two rings. These are modeled with our presented approach.

First, we define the specific reference kinematics, then we show the inherent properties of the ring model with numerical tests and finally we compare the results in the overall CVT system to the ones gained with different beam models.

5.1 Kinematics of the reference curve

The derived EOMs (25) are valid for any belt system with a planar reference curve. For the application within the CVT system, we have to choose the corresponding reference curve. We omit the index *ref* in this section for the sake of clearness. All kinematical values refer to the center line of the beam model. The reference curve consists of four parts which are depicted in Fig. 5:

– primary arc with radius r_P and length $b_P = 2r_P(\pi - \varphi)$,
– upper strand with length $b = d_A \cos\alpha$,
– secondary arc with radius r_S and with length $b_S = 2r_S\varphi$,
– lower strand with length b.

The relations $\alpha := \arcsin(\frac{r_S - r_P}{d_A})$ and $\varphi := \arccos(\frac{r_P - r_S}{d_A})$ are used. Denoting the geometric ratio (of the reference curve radii) by $i_g := \frac{r_S}{r_P}$, we define the scalar ratio parameter

$$\Theta := \frac{1 - i_g}{1 + i_g} \quad \Leftrightarrow \quad i_g = \frac{1 - \Theta}{1 + \Theta}.$$

This parameter is sufficient to describe the reference motion and will be used as degree of freedom for the global shape ($q_R = \Theta$).[4]

For a given geometric ratio Θ, the primary and secondary radii can be deduced using the fact that

$$0 = L - 2b - b_P - b_S.\tag{27}$$

Considering all the definitions outlined earlier, (27) provides a nonlinear relationship where d_A—the constant distance between the pulley axles—and L—the total length of the ring— are given geometrical properties of the CVT system. The changing transmission ratio as explicit DOF allows for the analysis of the dynamic behavior, e.g. in run-up phases [17, Chap. 5.2.2].

In a pre-processing step, the arc-radii for different Θ are computed solving the nonlinear system (27). The primary radius r_P is interpolated over the ratio parameter Θ with at least C^2-continuous splines. An explicit dependency $r_p(\Theta)$ results. The further kinematic description over the arc follows also explicitly and is C^1-continuous in ξ. For a given interpolated function of the primary radius $r_P(\Theta)$, the positional description for the upper part over the arc length ξ is given by

$$r^u = \begin{pmatrix} r_x^u \\ r_y^u \\ 0 \end{pmatrix} = \begin{cases} \begin{pmatrix} -r_S \cos(\varphi_S) \\ r_S \sin(\varphi_S) \\ 0 \end{pmatrix} & \text{if } 0 \le \xi \le \varphi r_S \\ r_{S,end} + \xi_T t_T & \text{if } \varphi r_S < \xi \le r_S \varphi + b \\ \begin{pmatrix} d_A - r_P \cos(\varphi_P) \\ r_P \sin(\varphi_P) \\ 0 \end{pmatrix} & \text{if } \varphi r_S + b \le \xi \le \frac{L}{2} \end{cases}\tag{28}$$

with the following definitions:

$$\varphi_S := \frac{\xi}{r_S}, \qquad \xi_T := \xi - r_S \varphi, \qquad \xi_P := \xi - r_S \varphi + b, \qquad \varphi_P := \varphi + \frac{\xi}{r_P},$$

$$r_{S,end} := \begin{pmatrix} -r_S \cos \varphi \\ r_S \sin \varphi \\ 0 \end{pmatrix} \quad \text{and} \quad t_T := \frac{r_{P,start} - r_{S,end}}{|r_{P,start} - r_{S,end}|}.$$

The lower part follows due to symmetry:

$$r^l(\xi) = \begin{pmatrix} r_x^u(\xi - L) \\ -r_y^u(\xi - L) \\ 0 \end{pmatrix}.\tag{29}$$

---

[4]The parameter Θ is defined in such a way that symmetric properties can be used in the numerical evaluation.

5.2 Trial functions

Finite elements, used to discretize the deformation around the reference configuration, are distributed along the entire length of the belt. Hermite interpolation trial functions are chosen to respect the prerequisite of C^1-continuity. In this example we focus on planar overlaid deformation and write

$$N_1 := \tfrac{1}{2} - \tfrac{3}{4}x + \tfrac{1}{4}x^3, \qquad N_2 := \tfrac{l_e}{8} - \tfrac{l_e}{8}x - \tfrac{l_e}{8}x^2 + \tfrac{l_e}{8}x^3,$$

$$N_3 := \tfrac{1}{2} + \tfrac{3}{4}x - \tfrac{1}{4}x^3, \qquad N_4 := \tfrac{l_e}{8} + \tfrac{l_e}{8}x - \tfrac{l_e}{8}x^2 - \tfrac{l_e}{8}x^3,$$

where l_e is the element length and $x \in [-1; 1]$ the local coordinate in the FE coordinate system. For each direction we introduce one DOF for the position [5] and one additional DOF for its derivative.[6] Four DOFs per node result. The local deformation within one finite element is therefore affected by in total eight DOFs which are interpolated by the interpolation matrix $\mathbb{S}^e$

$$\mathbb{S}^e = \begin{bmatrix} N_1 & N_2 & 0 & 0 & N_3 & N_4 & 0 & 0 \\ 0 & 0 & N_1 & N_2 & 0 & 0 & N_3 & N_4 \\ 0 & 0 & 0 & 0 & 0 & 0 & 0 & 0 \end{bmatrix}.$$

$\mathbb{S}_i$ is obtained after assembly of the element shape function $\mathbb{S}^e$.

5.3 Numerical tests

The equations are implemented in MBSim [21, 27] and tested qualitatively in the following. The first virtual experiment tests the dynamics of the reference kinematics only, i.e., $q_f = 0$. The parameters follow a real ring of a pushbelt CVT such that steel material and the geometrical properties are incorporated. The initial condition is for the DOFs $\Theta = 0.4$, $s = 0$ and $\dot{\Theta} = \dot{s} = 0$, i.e., an overdrive ratio of $i_g \approx 0.4286$ is set. Results are depicted in Fig. 6 for the deformation of the ring. Four different time points are given where t_0 is at the initial condition. At t_1 an intermediate state is given. One can see that the ratio changes over time and oscillates around the neutral state $\Theta = 0$. The parameter s stays zero up to numerical errors. Keeping in mind that the local deformations are blocked, this is the expected result.

For a general model with all DOFs, one would expect a circular shape as neutral state. Therefore, another experiment is performed with the same belt, but adding the local deformations, i.e., $q_f \neq 0$. As the local deformations are able to represent rigid body motion, the overall position is redundantly described taking into account also the reference DOFs.
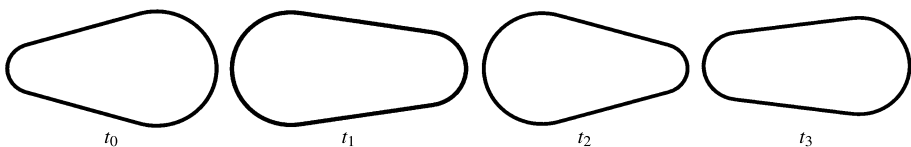

Fig. 6 Snapshots of reference oscillation ($q_f = 0$)

---

[5]Interpolated by N_1 and N_3.

[6]Interpolated by N_2 and N_4.

t_0 t_1 t_2 t_3
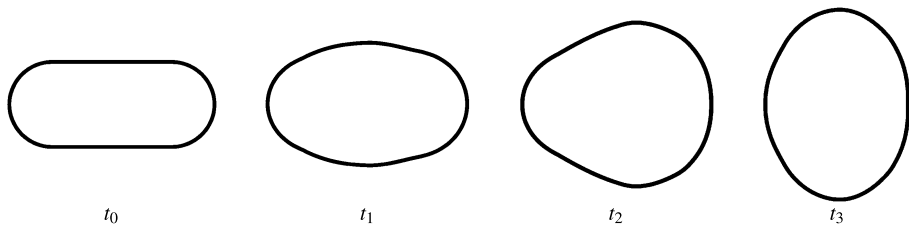
Fig. 7 Snapshots of a deformable ring with 8 FEs

As a consequence, the mass matrix becomes singular. Therefore, local DOFs q_f need to be locked. We fix one node to its reference position such that it moves only due to the reference coordinates within the xy-plane. We choose the first node for all simulations, which is at $\xi = 0$. The same settings as before are used. Eight FEs are used along the belt. All generalized positions and velocities satisfy $q = \dot{q} = 0$ at $t_0 = 0$.

Snapshots of the belt are depicted in Fig. 7 for four different times in chronological order. One can see that at t_1 the ring shows a reasonable behavior. Similar to a (rubber) band, it starts to form a circular shape. The strands deform outwards. At t_2 however, the belt exhibits a rather unexpected shape. The first node[7] can only move with the reference DOFs, i.e., Θ in this case. To form a circular shape, the left node has to move to the center, i.e., Θ increases. The typical shape of the CVT ring for $\Theta > 0$ can be seen, i.e. overdrive, as Θ influences the deformation over the whole arc. Yet, the deformation develops further yielding an oval-like shape again at t_3, which is the expected behavior.

With this second example we want to emphasize the following: The presented modeling strategy relies on the description of the reference curve. The model assumes an external force distribution that yields a shape similar to the one of the reference configuration. Only small deviations from the reference are incorporated correctly. This explains why the results obtained between t_0 and t_1 in the previous examples (Fig. 7) are as physically expected and why the shape computed at t_2 is an artifact of the chosen discretization. Nevertheless the small deformation behavior is quantitatively correct as can be seen from the shape computed at t_3.

5.4 Application

The numerical tests show particularly that our system relies on the application of external forces on it, which keep it close to its reference shape. In fact, the overlaid deformations are assumed to be small and can be interpreted as a linearization about the changing reference state. The model does not behave quantitatively correctly, when it is "far off" this state. Thus, the main application in mind is the simulation of a pushbelt CVT [17], whereby this section presents the results using the newly derived model and a comparison with other beam models which are implemented in MBSim [21, 27]. In total four beam models are used:

RCM It follows the co-rotational approach and is a planar implementation of the model of [13, 14, 41, 43]. In the simulation 32 FEs are used, which yields 160 DOFs.
ANCF It is the planar implementation of the ANCF-theory of [32]. Forty FEs yield 160 DOFs.

---

[7]Here on the left side of the ring.

Table 1 Nine load cases defined by the transmission ratio and the primary torque

	1	2	3	4	5	6	7	8	9
$i_g\,[-]$	0.47	1.00	2.42	0.47	1.00	2.42	0.47	1.00	1.30
$T_P\,[Nm]$	30	30	30	50	50	50	100	100	100

ALE0 It is the planar implementation of the present model without overlaid deformation. It only considers the two reference DOFs s and Θ.

ALE Compared to the ALE0 model it also considers overlaid deformations with 157 DOFs and 40 FEs.

In Sect. 3.1, we introduced two possibilities to choose the direction matrix $\mathbb{A}_i$. For the application within the CVT the simple option has proven to be most suitable, i.e., $\mathbb{A}_i$ is chosen to be the constant identity matrix. This results in less evaluated derivatives, reducing thereby the CPU time. In the general second possibility $\mathbb{A}_i$ would change at every time step as Θ does not stay constant but oscillates. The interpretation of the DOFs would change in every time step and the local DOFs would "see" the oscillations in Θ, resulting in a numerically unfavorable behavior. As introduced before, the small overlaid deformations are planar.

We draw different general conclusions comparing the results of nine different load cases (see Table 1). The loads are taken from measurements to ensure realistic settings. The belt speed has minor influence and is hold constant for the primary pulley with $\omega_P = 2000$ RPM. The transmission ratio is varied in three way, i.e. $i_g < 1$, $i_g \approx 1$ and $i_g > 1$. In the experiments the torques of $T_P^1 = 30$ Nm, $T_P^2 = 50$ Nm and $T_P^3 = 100$ Nm where applied on the primary pulley. At the primary pulley we ensure kinematically a constant distance to fix the transmission ratio. On the secondary pulley we apply torques and forces T_S^* and F_S^*, which are taken from measurements of a reference belt and which ensure safe operation. The measurements were conducted by ©Bosch Transmission Technology.

Thereby, the output with the RCM model is used as reference as it was successfully tested in prior work [7, 8, 13, 14]. The differences to the other models are evaluated by considering the thrust ratio i_F (Fig. 8a), which is the ratio between the two clamping forces at the pulley sheaves, as well as by analyzing a measure of efficiency η (Fig. 8b). It can be seen that all models converge globally to the same level, i.e., a similar thrust ratio and efficiency. Yet, the ALE0 model yields in overdrive[8] very high values for the thrust ratio whereas the ANCF model yields low values in medium[9] and underdrive[10] configurations. Furthermore, higher losses compared to the other models result when using the ANCF model.

Figure 8c reveals the reason for these discrepancies. Given are the push forces acting on one push element in longitudinal direction along one revolution for case 3. First these build up in the primary pulley arc. Then they are rather constant in the push-strand between the pulleys. In the secondary pulley arc they decrease again.

The ANCF model reacts very stiff. High oscillations result in the complete system as seen in the figure. For the efficiency computation, this means that many oscillations around a zero level (e.g. after $t = 0.08$ s) arise. It leads to errors within the numerical integration of the efficiency values. The ALE0 model deviates from the other three for what concerns spiral running[11] (Fig. 8d). As the model does not support local deformations along the belt

---

[8]Cases 1, 4 and 7.

[9]Cases 2, 5 and 8.

[10]Cases 3, 6 and 9.

[11]The pulley sheaves deform due to the clamping forces. Thus, elements change the running radius within a pulley arc, which is called spiral running.
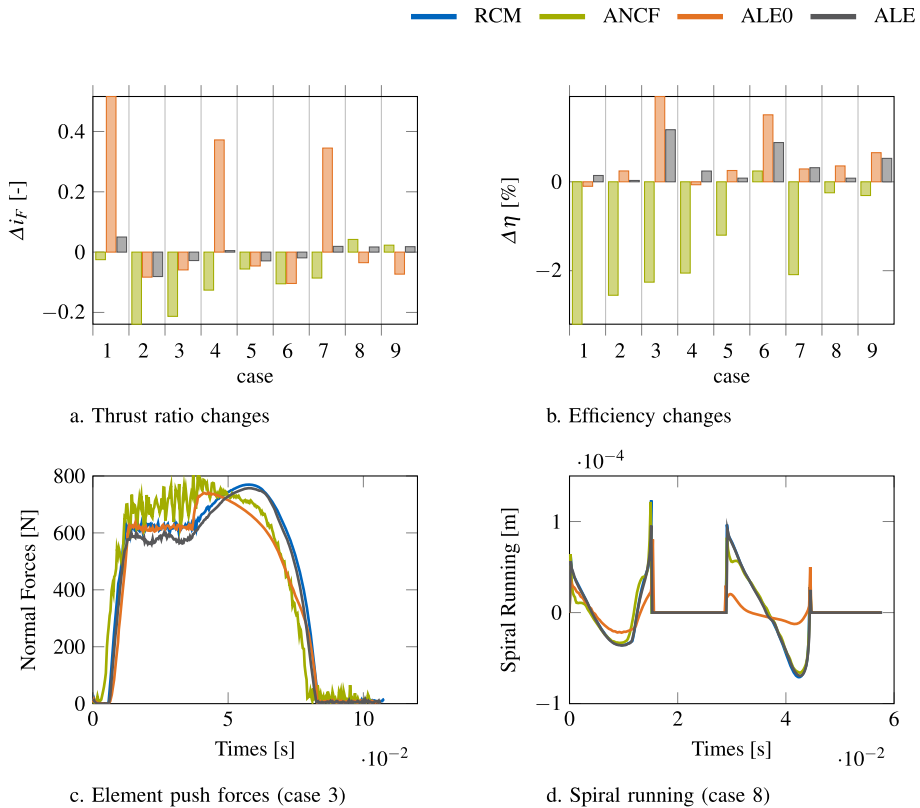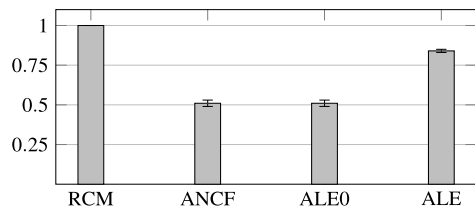
a. Thrust ratio changes

b. Efficiency changes

c. Element push forces (case 3)

d. Spiral running (case 8)

Fig. 8 Comparing different beam models. The results gained with the RCM model are used as reference

Fig. 9 Average CPU costs for beam models where RCM is the reference. The error bars show the maximum deviations from the average value

only a local stiffness in the contact enables small deviations from the circular arc. The pulley sheaves deform differently, which influences the axial force distribution along the arcs and therefore the thrust ratio.

For the nine cases, the computational times are compared in Fig. 9. Again the simulation times of the RCM model are used as reference. The error bars indicate the maximal deviation from the mean value. The ANCF and the ALE0 model take up only about the half of the simulation time. The computational time for the full simulation with the ALE approach takes only about 80% of the computation time with the reference RCM approach.

Altogether, the ALE model proves to be a good reference model. The simulation time is reduced ensuring a good correlation with an already validated RCM model. Depending on

the application, it is easy to adjust the level of detail[12] reducing the simulation times even further.

6 Summary

In this paper, we present a beam model based on planar geometrically nonlinear reference dynamics which is described by actual degrees of freedom of the model and we add overlaid spatial deflections. The derivation is based on the small strain assumption and makes use of the Arbitrary Lagrangian Eulerian transformation. Hence, we deal with both periodic motion, which can be reduced due to the Eulerian view, and contact conditions, which are represented by the Lagrangian view. The planar large reference motion may change the shape dynamically, which is a significant extension to models from literature. The original application of the derivation is a large spatial model for pushbelt continuously variable transmissions. The idea—known from e.g. the floating frame of reference method—is to describe the nonlinear reference motion and additional small deviations separately. We show that the new model represents the phenomena even better than the previous models or in a comparable way, and that it saves computational time. Hence, the contribution of the paper is twofold: theoretically as there is no model with changing reference shape in the literature; practically as it allows for efficient and reliable spatial simulation of pushbelt CVTs for the first time.

7 Further considerations

Based on the summary, we propose to answer the following questions for future work.

– Application to other belt systems
  The presented approach is not restricted to the pushbelt CVT. It can be used for any belt system with a closed one-dimensional curve and a reference kinematics.
– Separated integration
  The separation of the reference curve and the overlaid deformation enables the possibility to separate these DOFs for the numerical integration. This makes sense, if e.g. the reference DOFs change only slowly compared to the overlaid deformations and so they need not to be updated in every time step. This reduces the simulation costs and increases the robustness of the overall simulation model as the dynamical coupling of the DOFs is weakened.
– Model reduction
  A nonlinear model order reduction technique, e.g., the proper orthogonal decomposition (POD), is necessary to reduce the computational effort for the CVT application in the Lagrangian view. The coupling of the overall motion with local small deformation is the reason why both motions have to be identified at the same time. The Eulerian view in combination with the reference curve description offers the possibility to apply linear model order reduction techniques only to the overlaid deformations.
– Quasi-static overlaid deformation field
  The evaluation of the integrals with respect to the trial functions is time consuming and yields the most computational cost. For an overall good approximation, the reference

---

[12]For instance ALE0.

DOFs suffice to give good results (Fig. 8). However, the spiral running in the arcs is not represented which results in small deviations. From the overall state of the variator, it is possible to approximate the kinematics of the ring. The small deviations could be defined as quasi-static. Besides the spiral running, this idea can be adapted for the misalignment. The axial deviations of the rings can be deduced from the sheave positions as is done for the initialization in [26]. In both cases, the stiff behavior needs not be treated dynamically, which saves computational costs by adding spiral running and misalignment to the reference DOFs.

Publisher's Note   Springer Nature remains neutral with regard to jurisdictional claims in published maps and institutional affiliations.

References

1. Acary, V., Brogliato, B.: Numerical Methods for Nonsmooth Dynamical Systems: Applications in Mechanics and Electronics, 1st edn. Lecture Notes in Applied and Computational Mechanics, vol. 35. Springer, Berlin (2008)
2. Antman, S.: Nonlinear Problems of Elasticity. Springer, Berlin (2005)
3. Bathe, K.J., Bolourchi, S.: Large displacement analysis of three-dimensional beam structures. Int. J. Numer. Methods Eng. **14**, 961–986 (1979)
4. Bauchau, O.: Flexible Multibody Dynamics. Springer, Berlin (2010)
5. Behdinan, K., Tabarrok, B.: Dynamics of flexible sliding beams – non-linear analysis part II: transient response. J. Sound Vib. **208**(4), 541–565 (1997). https://doi.org/10.1006/jsvi.1997.1168. http://www.sciencedirect.com/science/article/pii/S0022460X97911688
6. Belytschko, T., Schwer, L.: Large displacement, transient analysis of space frames. Int. J. Numer. Methods Eng. **11**, 65–84 (1977)
7. Cebulla, T.: Spatial dynamics of pushbelt cvts: model enhancements to a non-smooth flexible multibody system. Ph.D. thesis, Technische Universität München (2014)
8. Cebulla, T., Grundl, K., Schindler, T., Ulbrich, H., van der Velde, A., Pijpers, H.: Spatial dynamics of pushbelt CVTs: model enhancements. In: SAE Technical Paper of SAE World Congress, Detroit, 24th–26th April 2012 (2012)
9. Crisfield, M.A.: A consistent co-rotational formulation for non-linear, three-dimensional, beam elements. Comput. Methods Appl. Mech. Eng. **81**, 131–150 (1990)
10. von Dombrowski, S., Schwertassek, R.: Analysis of large flexible body deformation in multibody systems using absolute coordinates. In: Advances in Computational Multibody Dynamics, Lisbon, 20th–23rd September 1999, pp. 359–378. Instituto Superior Tecnico, Lisbon (1999).
11. Dufva, K., Kerkkänen, K., Maqueda, L.G., Shabana, A.A.: Nonlinear dynamics of three-dimensional belt drives using the finite-element method. Nonlinear Dyn. **48**(4), 449–466 (2007). https://doi.org/10.1007/s11071-006-9098-9. https://link.springer.com/article/10.1007/s11071-006-9098-9
12. Funk, K.: Simulation eindimensionaler Kontinua mit Unstetigkeiten. In: Fortschrittberichte VDI: Reihe 18, Mechanik, Bruchmechanik, vol. 294. VDI Verlag, Düsseldorf (2004)
13. Geier, T.: Dynamics of Push Belt CVTs, Fortschrittberichte VDI: Reihe 12, Verkehrstechnik, Fahrzeugtechnik, vol. 654. VDI Verlag, Düsseldorf (2007)
14. Geier, T., Förg, M., Zander, R., Ulbrich, H., Pfeiffer, F., Brandsma, A., van der Velde, A.: Simulation of a push belt CVT considering uni- and bilateral constraints. J. Appl. Math. Mech. **86**, 795–806 (2006)
15. Geradin, M., Cardona, A.: Flexible Multibody Dynamics: A Finite Element Approach. Wiley, New York (2001)
16. Gerstmayr, J., Sugiyama, H., Mikkola, A.: An overview on the developments of the absolute nodal coordinate formulation. In: Proceedings of 2nd Joint International Conference on Multibody System Dynamics, Stuttgart, 29th May–1st June 2012 (2012)
17. Grundl, K.: Validation of a pushbelt variator. Ph.D. thesis, Technische Universität München (2015)
18. Irschik, H., Holl, H.: The equations of Lagrange written for a non-material volume. Acta Mech. **153**, 231–248 (2002)
19. Jelenic, G., Saje, M.: A kinematically exact space finite strain beam model – finite element formulation by generalized virtual work principle. Comput. Methods Appl. Mech. Eng. **120**(1), 131–161 (1995). http://www.sciencedirect.com/science/article/pii/004578259400056S

20. Lang, H., Linn, J., Arnold, M.: Multi-body dynamics simulation of geometrically exact Cosserat rods. Multibody Syst. Dyn. **25**(3), 285–312 (2011)
21. MBSim – multi-body simulation software. GNU Lesser General Public License. https://github.com/mbsim-env/
22. Pechstein, A., Gerstmayr, J.: A Lagrange–Eulerian formulation of an axially moving beam based on the absolute nodal coordinate formulation. Multibody Syst. Dyn. **30**(3), 343–358 (2013). http://link.springer.com/article/10.1007/s11044-013-9350-2
23. Pfeiffer, F.: Mechanical System Dynamics, corr. 2nd printing edn. Lecture Notes in Applied and Computational Mechanics, vol. 40. Springer, Berlin (2008)
24. Pfeiffer, F., Schindler, T.: Introduction to Dynamics. Springer, Berlin (2015)
25. Romero, I.: A comparison of finite elements for nonlinear beams: the absolute nodal coordinate and geometrically exact formulations. Multibody Syst. Dyn. **20**, 51–68 (2008)
26. Schindler, T.: Spatial Dynamics of Pushbelt CVTs. In: Fortschritt-Berichte VDI: Reihe 12, Verkehrstechnik, Fahrzeugtechnik, vol. 730. VDI Verlag, Düsseldorf (2010). http://mediatum.ub.tum.de/node?id=981870
27. Schindler, T., Förg, M., Friedrich, M., Schneider, M., Esefeld, B., Huber, R., Zander, R., Ulbrich, H.: Analysing dynamical phenomenons: introduction to MBSim. In: Proceedings of 1st Joint International Conference on Multibody System Dynamics, Lappeenranta, 25th–27th May 2010 (2010)
28. Schindler, T., Friedrich, M., Ulbrich, H.: Computing time reduction possibilities in multibody dynamics. In: Blajer, W., Arczewski, K., Fraczek, J., Wojtyra, M. (eds.) Multibody Dynamics: Computational Methods and Applications, Computational Methods in Applied Sciences, vol. 23, pp. 239–259. Springer, Dordrecht (2011)
29. Schindler, T., Geier, T., Ulbrich, H., Pfeiffer, F., van der Velde, A., Brandsma, A.: Dynamics of pushbelt CVTs. In: Umschlingungsgetriebe: Ketten und Riemen – Konstruktion, Simulation und Anwendung von Komponenten und Systemen, Tagung Berlin, 21. und 22. Juni 2007, VDI-Berichte. VDI Verlag, Düsseldorf (2007).
30. Schindler, T., Ulbrich, H., Pfeiffer, F., van der Velde, A., Brandsma, A.: Spatial simulation of pushbelt CVTs with timestepping schemes. Appl. Numer. Math. **62**(10), 1515–1530 (2012)
31. Schwertassek, R., Wallrapp, O.: Dynamik Flexibler Mehrkörpersysteme. Vieweg, Wiesbaden (1999)
32. Shabana, A.: Dynamics of Multibody Systems, 3rd edn. Cambridge University Press, New York (2005)
33. Shabana, A.A.: Flexible multibody dynamics: Review of past and recent developments. Multibody Syst. Dyn. **1**(2), 189–222 (1997). https://doi.org/10.1023/A:1009773505418
34. Simo, J.: A finite strain beam formulation. The three-dimensional dynamic problem. Part I. Comput. Methods Appl. Mech. Eng. **49**(1), 55–70 (1985). https://doi.org/10.1016/0045-7825(85)90050-7
35. Simo, J., Vu-Quoc, L.: A three-dimensional finite-strain rod model. Part II: computational aspects. Comput. Methods Appl. Mech. Eng. **58**(1), 79–116 (1986). https://doi.org/10.1016/0045-7825(86)90079-4
36. Sonneville, V., Cardona, A., Brüls, O.: Geometrically exact beam finite element formulated on the special Euclidean group. Comput. Methods Appl. Mech. Eng. **268**, 451–474 (2014). https://doi.org/10.1016/j.cma.2013.10.008
37. Vetyukov, Y.: Mechanics of axially moving structures at mixed Eulerian-Lagrangian description. In: Analysis and Modelling of Advanced Structures and Smart Systems, Advanced Structured Materials. Springer, Singapore (2018). https://doi.org/10.1007/978-981-10-6895-9_13. https://link.springer.com/chapter/10.1007/978-981-10-6895-9_13
38. Vetyukov, Y.: Non-material finite element modelling of large vibrations of axially moving strings and beams. J. Sound Vib. **414**, 299–317 (2018). https://doi.org/10.1016/j.jsv.2017.11.010. http://linkinghub.elsevier.com/retrieve/pii/S0022460X17307824
39. Vu-Quoc, L., Li, S.: Dynamics of sliding geometrically-exact beams: large angle maneuver and parametric resonance. Comput. Methods Appl. Mech. Eng. **120**(1–2), 65–118 (1995). https://doi.org/10.1016/0045-7825(94)00051-N
40. Wasfy, T., Noor, A.: Computational strategies for flexible multibody systems. Appl. Mech. Rev. **56**, 553–613 (2003)
41. Zander, R.: Flexible multi-body systems with set-valued force laws. Fortschritt-Berichte VDI: Reihe 20, Rechnerunterstützte Verfahren, vol. 420. VDI Verlag, Düsseldorf (2009). http://mediatum2.ub.tum.de/node?id=654788
42. Zander, R., Rettig, F., Schindler, T.: Concepts for the simulation of belt drives – industrial and academic approaches. In: Proceedings of 1st Joint International Conference on Multibody System Dynamics, Lappeenranta, 25th–27th May 2010 (2010)
43. Zander, R., Ulbrich, H.: Reference-free mixed FE-MBS approach for beam structures with constraints. Nonlinear Dyn. **46**, 349–361 (2006)